Environment International 164 (2022) 107272

Contents lists available at ScienceDirect

Environment International

journal homepage: www.elsevier.com/locate/envint

Full length article

A new laser device for ultra-rapid and sustainable aerosol sterilization

Roman Vuerich [a,b], Valentina Martinelli [c], Simone Vodret [a], Iris Bertani [d], Tea Carletti [e], Lorena Zentilin [f], Vittorio Venturi [d], Alessandro Marcello [e], Serena Zacchigna [a,g,*]

[a] Cardiovascular Biology Laboratory, International Centre for Genetic Engineering and Biotechnology (ICGEB), 34149 Trieste, Italy
[b] Department of Life Sciences, University of Trieste, 34127 Trieste, Italy
[c] Eltech K-Laser s.r.l., 31100 Treviso, Italy
[d] Laboratory: Bacteriology Laboratory, International Centre for Genetic Engineering and Biotechnology (ICGEB), 34149 Trieste, Italy
[e] Molecular Virology Laboratory, International Centre for Genetic Engineering and Biotechnology (ICGEB), 34149 Trieste, Italy
[f] Molecular Medicine Laboratory, International Centre for Genetic Engineering and Biotechnology (ICGEB), 34149 Trieste, Italy
[g] Department of Medical, Surgical and Health Sciences, University of Trieste, 34127 Trieste, Italy

ARTICLE INFO

Handling Editor: Adrian Covaci

Keywords:
Laser light
Aerosol
SARS-CoV-2
Legionella pneumophila
Air sterilization

ABSTRACT

The current COVID-19 pandemic has highlighted the importance of aerosol-based transmission of human pathogens; this therefore calls for novel medical devices which are able to sterilize contaminated aerosols. Here we describe a new laser device able to sterilize droplets containing either viruses or bacteria. Using engineered viral particles, we determined the 10,600 nm wavelength as the most efficient and exploitable laser source to be manufactured in a commercial device. Given the lack of existing working models to reproduce a human aerosol containing living microbial particles, we developed a new system mimicking human droplet formation and preserving bacterial and viral viability. This evidenced the efficacy of 10,600 nm laser light to kill two aerosol transmitted human pathogens, *Legionella pneumophila* and SARS-CoV-2. The minimal exposure time of <15 ms was required for the inactivation of over 99% pathogens in the aerosol; this is a key element in the design of a device that is safe and can be used in preventing inter-individual transmission. This represents a major advantage over existing devices, which mainly aim at either purifying incoming air by filters or sterilizing solid surfaces, which are not the major transmission routes for airborne communicable diseases.

1. Introduction

After two years from the start of the current COVID-19 pandemic, the sanitary and social impact of airborne diseases is very evident (Zacchigna et al., 2021). The development of several vaccines is playing a major role in the control of the epidemic, however quarantine of infected individuals is still the major method used to control aerosol transmission, with clear economic implications (Pak et al., 2020). This is largely due to the lack of effective devices that can be placed between people, particularly in closed spaces, and are able to clean the air contaminated by infected individuals. Different from filters, such a device should ideally sterilize the air as infected people enter in the room, thus significantly restricting inter-individual transmission.

Existing technologies to prevent transmission of respiratory human pathogens such as SARS-CoV-2, can be generally classified into four main categories. The most common category consists of high efficiency particulate air (HEPA) filters, which mechanically remove > 99% of dust, pollen, mold, bacteria, and any airborne particles >0.3 μm (Lippi et al., 2022). Despite this high efficiency in air cleaning, filters require periodic replacement in order to function properly. In addition, filters themselves can shelter viable microbes and support their growth, particularly under high humidity (Pasanen et al., 1993). In addition, used filters requires specific disposal, with associated costs and risk of environmental contamination (Lippi et al., 2022). Another limitation of these filters is that they can only purify the air when it is introduced into a closed space and not after the entrance of infected individuals. Another common type of air sterilizers are electric discharge devices, which either induce air ionization (electrophysical effect) or produce ozone (electrochemical effect) (Wang et al., 2019). Ozone, which is highly toxic for both humans and animals, is also formed as a byproduct of the electrophysical effect, which limits the applicability of these devices in close environments (Volker et al., 2019). Often used sterilizing systems

* Corresponding author at: Cardiovascular Biology, International Centre for Genetic Engineering and Biotechnology (ICGEB), Padriciano, 99, 34149 Trieste, Italy.
E-mail address: zacchign@icgeb.org (S. Zacchigna).
URL: https://www.icgeb.org/cardiovascular-biology/ (S. Zacchigna).

https://doi.org/10.1016/j.envint.2022.107272
Received 23 March 2022; Received in revised form 27 April 2022; Accepted 27 April 2022
Available online 2 May 2022

exploit ultraviolet (UV) light, which involves wavelengths ranging from 100 to 400 nm, and in particular UVC (200–280 nm) (Kim and Kang, 2018). UVC radiation is mainly produced by mercury lamps and light-emitting diodes (LEDs), which have limitations. Mercury lamps are highly pollutant, they have a limited lifetime and need some time to be switched and become operative. UV generating LEDs on the other hand have several advantages, as they are compact, work at a low voltage and immediately turn on (Buse et al., 2022). Yet, they are under-developed in the UVC range (they are most often used to generate UVB) and are more expensive than mercury lamps (Gora et al., 2019). In addition, UV irradiation is dangerous for human health, particularly for the skin and the eye. Finally, photocatalytic systems can also be employed in air purification technologies (Ren et al., 2017). Semiconductor materials, such as titanium dioxide (TiO_2) or zinc oxide (ZnO), are activated by light ranging from UV to the near infrared spectrum, and thereby result in the production of reactive oxygen species (ROS) (Smijs and Pavel, 2011). ROS damage biomolecules and thus efficiently inactivate living microbes (Fasnacht and Polacek, 2021; Rupel et al., 2018). In this case, the optimal anti-microbial activity must be established for each micro-organism by tuning the irradiation time, which can vary from minutes to hours (Bono et al., 2021; Feng et al., 2017; Matsuura et al., 2021). These materials are often sprayed on top of non-HEPA filters and used in combination with UV light (Eisenloffel et al., 2019). In addition to the relatively long exposure time, another limitation of photocatalytic materials is the use of UV lamps for their activation, with already mentioned UV-associated disadvantages.

Different from all these systems, laser light is emerging as a novel option to destroy both viruses and bacteria. Compared to other light sources, laser offers the advantage of higher average power, lower cost and greater reliability (Buffolo et al., 2021). In addition, laser light is monochromatic, coherent, and unidirectional, which allows the selection of the optimal wavelength to exert a specific biological effect. We and others have shown that blue laser light can be exploited to inactivate bacterial pathogens, for example on infected wounds (Rupel et al., 2019). Yet, the potential use of laser light to sterilize a contaminated aerosol has never been reported. Here, we describe the generation of a new laser device able to inactivate over 99% of aerosolized viral and bacterial pathogens in a very short time (<15 ms). This device exploits infrared light, and in particular the mid infrared (MIR) region, from 3000 to 12,000 nm. This range corresponds to the absorption of vibrational transitions of molecules, which are the frequencies at which interatomic bonds typically oscillate. Absorption of MIR light by vibrational transition leads to photothermal effect, by which the energy deposited in a vibrational bond quickly spreads to adjacent bonds, increasing the temperature of the molecule (Chikkaraddy et al., 2022; Tsai and Hamblin, 2017). This in turn, results in photodamage, for example protein misfolding, or, in extreme cases, in bond breaking and decomposition of the molecule (Hawkins and Davies, 2019).

2. Material and methods

2.1. Adeno-Associated Virus (AAV) vector production

AAV6 vectors (herein referred as AAV) were produced by the AAV Vector Facility at ICGEB Trieste, according to established procedures (Eulalio et al., 2012; Zacchigna et al., 2018). Briefly, infectious AAV particles expressing the Enhanced Green Fluorescent Protein (EGFP) were generated in HEK293 cells using the AAV Helper Free Packaging System (Cellbiolabs, #VPK-402). Viral stocks were obtained by $CsCl_2$ gradient centrifugation and titrated by quantifying the number of viral genomes (vg) per ml by real-time PCR, as described (Eulalio et al., 2012; Zacchigna et al., 2018).

2.2. LentiViral (LV) vector production

LV particles were produced by transient calcium phosphate transfection of HEK293 cells with the following plasmids: (i) transfer vector pLVTHM (Addgene, #12247), coding for EGFP (ii) expression vector pMD-VSVG, coding for the Vesicular Stomatitis Virus-G (VSV-G) envelope protein, and (iii) the PsPAX packaging plasmid. Lentiviral concentrator (Origene, TR30025) was used to concentrate LV particles. Viral titer was quantified by calculating the number of infectious units (iu) per ml by adding serial dilutions of the viral stock to HEK293 cells and quantifying the percentage of $EGFP^+$ fluorescent cells. Titration was validated using commercial LV particles (Santa Cruz Biotechnology, #sc-108084).

2.3. Laser irradiation in static conditions

1 µl drops of both AAV (5×10^{12} vg/ml) and LV (5×10^6 iu/ml) preparations were spotted in different wells of a 96-well plate. Wells were irradiated for 2 s using 445 nm, 970 nm, 1940 nm and 10,600 nm laser light at variable distances (1 cm, 10 cm and 50 cm). All laser devices were provided by Eltech K-laser. Laser parameters are described in Supplementary Table 1. Then, 5000 HEK293 cells were seeded in both treated and non-treated wells. After 48 h cell nuclei were stained with Hoechst 33,342 (Invitrogen, #H3570) diluted 1:20,000 in phosphate buffered saline (PBS) for 10 min before imaging. Efficiency of transduction by each vector type was quantified by measuring EGFP expression by HEK293 cells and by staining cellular nuclei with the blue dye Hoechst. Ten images were acquired per biological replicate ($n \geq 4$) and quantified the $EGFP^+$ area (green pixels) in each image. This number was divided for the number of blue pixels, thus normalizing the level of EGFP expression on the number of cellular nuclei in each image.

2.4. Generation of a new nebulizer preserving microbial viability

We modified a commercially available nebulizer device, exploiting Venturi effect (Nebula, Air Liquide Healthcare). In our system, the Venturi effect was operated by a piston pump, controlled by an electric duty cycle motor, powered by a square wave (and therefore not in continuous wave), operating at 3 Hz with 41% duty cycle. The insertion of a 2 m long silicone tube as a low pass filter allowed to keep a constant airflow at the inlet and to produce 0.6 m/s air speed at the outlet of the aerosol dispenser. Details on all components are provided as Supplementary Material.

2.5. Nebulization of LV vector using our and commercially available nebulizers

a 3 ml Dulbecco's modified Eagle medium (DMEM), 2% fetal bovine serum (FBS) solution containing 5×10^6 iu/ml LV particles was nebulized using either our nebulizer (detailed information is provided in Supplementary Material), a vacuum pump connected with a liquid dispenser (Nebula, Air Liquide Healthcare), or two commercially available nebulizers, producing aerosol droplets exploiting ultrasounds (Laica MD6026) and Venturi effect (Nebula, Air Liquide Healthcare). After aerosol condensation, 20 µl of LV particles were eventually added to 5000 HEK293 cells seeded in a 96-well plate. After 48 h cells were incubated with Hoechst and the $EGFP^+$ area was quantified to assess the activity of viral particles.

2.6. SARS-CoV-2 production and plaque assay

All experiments with SARS-CoV-2 were conducted in the Biosafety Laboratory Level 3 of the International Centre for Genetic Engineering and Biotechnology (ICGEB) in Trieste (Italy). Vero E6 cells (ATCC, #1586) were grown under standard conditions in DMEM supplemented with 10% FBS and antibiotics. Cells were maintained at 37 °C under 5% CO_2 and routinely tested to exclude mycoplasma contamination. Working stocks of SARS-CoV-2 (isolate FVG_ICGEB_isolated and sequenced in ICGEB, Trieste (Licastro et al., 2020) were routinely

propagated and titrated on Vero E6 cells up to passage 4. Plaque assay was performed by incubating dilutions of SARS-CoV-2 on Vero E6 monolayers at 37 °C for 1 h, as previously described (Rajasekharan et al., 2021). Briefly, cells were washed with PBS and overlaid with DMEM, 2% FBS, 1.5% carboxymethylcellulose (Sigma Aldrich, #c5678) for 3 days. Cells were eventually stained with crystal violet 1%. Plaques were manually counted and multiplied by the dilution factor to determine viral titer, expressed as plaque-forming units (pfu)/ml.

2.7. Laser irradiation in aerosol conditions

A 3 ml solution containing 5×10^6 iu/ml LV particles or human pathogens *L. pneumophila* and SARS-CoV-2 (stock concentration is reported in Tables 1 and 2) were nebulized using our nebulizer and exposed to 10,600 nm laser light, as detailed in Supplementary Material. Condensed aerosol (20 μl) of LV was added to 5000 HEK293 cells seeded in a 96-well plate, followed by evaluation of laser effect as explained for static conditions. Activity of laser light on SARS-CoV-2 was evaluated by plaque assay as described above. Viability of *L. pneumophila* was assessed quantifying the colony forming units (cfu) in control conditions and upon exposure of the aerosol to laser treatment (Allegra et al., 2016). Briefly, a suspension of *L. pneumophila* was divided into two parts and separately aerosolized. The first aerosol was exposed to laser, while the second one was used as untreated control. Condensed aerosol (200 μl) was serially diluted up to 10^{-4}. For each dilution, five spots (20 μl each) were made on *Legionella* agar base supplemented with BCYE Growth Supplement (Oxoid Limited, #CM0655 and #SR0110) plates. Plates were then tilted to allow droplet flow and incubated at 37 °C for 24 h. Where possible, the number of cfu was counted in each column and related to the volume spotted and the dilution factor applied in the same plate. This allowed the calculation of viable cfu/ml in the bacterial suspension condensed from both control and laser-treated aerosols.

2.8. Harvesting of human aerosol from a speaking individual

The aerosol of a speaking individual was collected on a cell culture dish, placed at 20 cm from the mouth. The person was loudly speaking for 15 s. The droplets of the aerosol deposited on the plate were imaged by bright-field microscopy including a micrometric ruler in the image. The diameter of at least 500 droplets was measured. Samples were collected upon acquisition of individual informed consent and approval by the competent ethical committee (authorization n. 103_2020H, 11/10/2021).

2.9. Imaging

Fluorescence images for the quantification of EGFP expression upon AAV and LV transduction were acquired using a Nikon Eclipse Ti-E inverted fluorescent microscope equipped with a DC-152Q-C00-FI camera using the NIS V4.30 software (Nikon). Bright-field images for droplet size quantification were acquired using Leica inverted microscope equipped with Leica DFC450 C camera using LAS V4.4 software (Leica Microsystems). Images were processed and analyzed using Fiji software (NIH, Bethesda).

Table 1
Quantification of SARS-CoV-2 viral titre by plaque assay in the original stock (input) and in the condensed aerosol harvested from control tank n. 8 (CTRL) and laser tank n. 5 (LASER) of our prototype. The efficiency of inactivation is indicated for each experiment, together with its average and standard deviation.

	INPUT	CTRL	LASER	Inactivation (%)
Exp 1	6×10^5 pfu/ml	6×10^5 pfu/ml	1.8×10^3 pfu/ml	99.70
Exp 2	6×10^5 pfu/ml	4×10^5 pfu/ml	3×10^2 pfu/ml	99.93
Exp 3	6×10^5 pfu/ml	6×10^5 pfu/ml	2×10^3 pfu/ml	99.67
			Average	**99.76**
			Standard deviation	**0.14**

Table 2
Quantification of viable *L. pneumophila* cfu/ml in the original stock (input) and in the condensed aerosol harvested from control tank n. 8 (ctrl) and laser tank n. 5 (laser) of our prototype. The efficiency of inactivation is indicated for each experiment, together with its average and standard deviation.

	INPUT	CTRL	LASER	Inactivation (%)
Exp 1	1.4×10^7 cfu/ml	2.92×10^6 cfu/ml	4.46×10^3 cfu/ml	99.85
Exp 2	1.4×10^7 cfu/ml	2.60×10^6 cfu/ml	4.43×10^3 cfu/ml	99.83
Exp 3	1.5×10^8 cfu/ml	6.17×10^6 cfu/ml	7.90×10^4 pfu/ml	98.72
Exp 4	1.5×10^8 cfu/ml	2.75×10^6 cfu/ml	7.70×10^4 pfu/ml	97.20
Exp 5	1.5×10^8 cfu/ml	4.30×10^7 cfu/ml	2.32×10^5 pfu/ml	99.46
Exp 6	1.5×10^8 cfu/ml	4.15×10^7 cfu/ml	2.46×10^5 pfu/ml	99.41
			Average	**99.01**
			Standard deviation	**1.01**

2.10. Statistical analysis

Three independent experiments in triplicates were performed for each condition. Average values are shown with the standard deviation and p-values. Statistical analysis was performed using GraphPad Prism 8.0. Unpaired student's *T*-test and One-Way ANOVA with Student-Newman-Keuls correction were used to determine statistical significance for normally distributed datasets, whereas non-normally distributed datasets were analyzed by ANOVA on ranks and Mann-Whitney *U* test. A p-value < 0.05 was considered statistically significant.

3. Results

3.1. Invisible infrared laser light efficiently inactivates both non-enveloped and enveloped viral particles

To evaluate the antimicrobial potential of multiple laser wavelengths, we made use of engineered viral vectors encoding for the EGFP reporter protein. AAV vectors were used, which are small, non-enveloped particles. LV vectors were also used, which, on the other hand, are larger and contain a lipid envelope (Fig. 1**a**). As described in Fig. 1**b, a** drop containing either AAV or LV particles was exposed to laser light, followed by seeding of HEK293 cells on top of the drop. We first compared the effect of two wavelengths that are commonly used in laser-based medical applications, namely 445 nm blue light, known to exert potent anti-microbial activity (Rupel et al., 2019), and 970 nm near infrared (NIR) light, commonly used in photobiostimulation (Ottaviani et al., 2013). We also tested 1940 nm short-wavelength (into the NIR as well) and the farer 10,600 nm MIR wavelength light, known to exert high photothermal effect. First, we assessed whether the distance between the laser source and the biological sample could impact the inactivation efficiency, by measuring the irradiance at 1, 10 and 50 cm from the laser source with a power meter. As expected for a coherent laser beam of only 1.2 mrad of divergence, the irradiance did not significantly change at the various distances. It was decided to perform experiments by placing the laser source at 50 cm from the biological sample, which represents the highest theoretical distance between the laser source and the pathogens in the device, as detailed later.

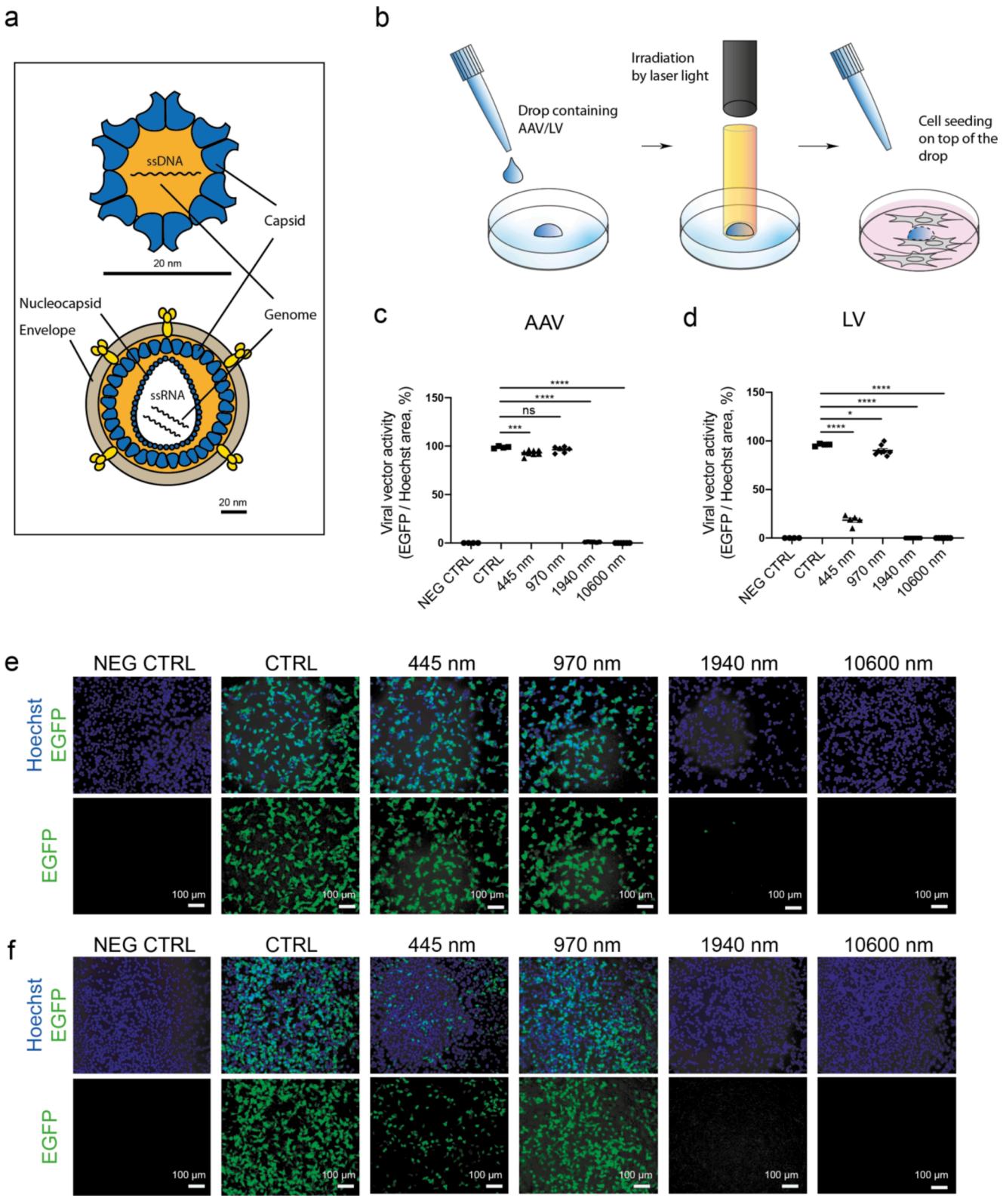

Fig. 1. Identification of the most effective laser wavelength in inactivating AAV and LV vectors, a. Schematic representation of an Adeno-Associated Virus (upper image) and a Lentivirus (lower image). **b.** Schematic representation of the experimental procedure used to compare the effect of multiple laser wavelengths on both AAV and LV vector transduction efficiency. **c, d.** Quantification of viral vector activity (defined as the ratio between $EGFP^+$ green area and $Hoechst^+$ nuclear area) upon transduction of HEK293 cells with a drop of either AAV-EGFP (1×10^6 vg/cell) or LV-EGFP (1×10^3 iu/cell) vectors in control conditions (CTRL) or exposed to the indicated laser wavelengths for 2 s. * $P < 0.05$; *** $P < 0.001$; **** $P < 0.0001$. Cells not exposed to any vector represent the negative control (NEG CTRL). The lower detection threshold in this assay is 10^4 vg/cell and 10 iu/cell for AAV and LV, respectively (**Supplementary** Fig. 1). **e, f.** Representative images of HEK293 cells corresponding to the graphs in panels **c** and **d**.

We then determined the sensitivity of the assay, by spotting 1 µl drop of both AAV-EGFP and LV-EGFP preparations at serial dilutions (1, 1:10, 1:100, 1:1000, 1:10,000) in different wells of a 96-well plate, followed by seeding of 5000 HEK293 cells. The efficiency of cell transduction by either viral vector was quantified by measuring EGFP expression and normalizing this result on the number of nuclei, stained by Hoechst. The ratio between EGFP area and Hoechst area can therefore be used as a surrogate for the number of EGFP^{+} transduced cells over the total number of cells. As shown in Supplementary Fig. 1, this allowed us to determine the lower detection threshold of our assay, corresponding to

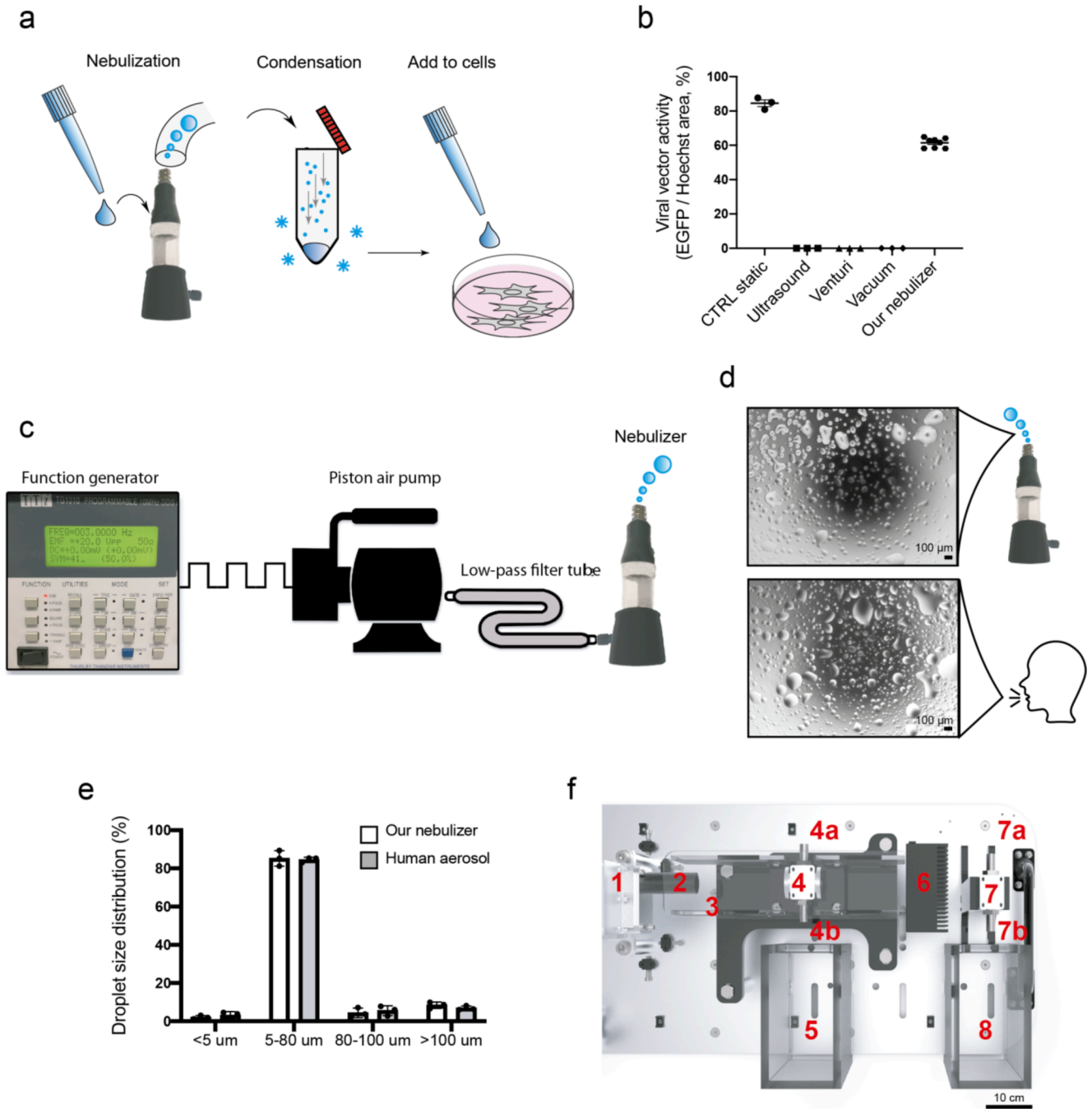

Fig. 2. Generation of a new nebulizer and laser device capable of sterilizing human-like aerosol contaminated by LV particles, a. Schematic representation of the experimental setup to evaluate LV vector activity upon nebulization with multiple commercial and custom systems. **b.** Quantification of LV-EGFP activity after nebulization. Multiple aliquots of the same LV-EGFP preparation were aerosolized using multiple systems, which exploit ultrasounds, Venturi effect and vacuum, as well as with our new nebulizer. The same volume of the generated aerosol was condensed by cooling and transferred to HEK293 cells. The lower detection threshold in this assay is 10 LV-EGFP iu/cell. **c.** Schematic representation of our nebulizer, in which a function generator operates at 3 Hz with 41% duty cycle to activate a piston air pump. A low-pass filter tube keeps a constant airflow, attenuated in pression. **d.** Representative images of an aerosol generated by our nebulizer (upper panel) and by a speaking individual. **e.** Distribution of droplet size generated by either our nebulizer or a speaking individual. **f.** Schematic representation of our laser prototype assembled with the new nebulizer. The aerosol was either exposed to laser for 12.5 ms or directly threw into the cooling tank for condensation. 1. Laser source; 2. Beam expander 5X; 3. Safety cover; 4. Laser chamber; 4a Aerosol inlet; 4b. Aerosol outlet; 5. Cooling tank for treated aerosol condensation; 6. Head power meter (which blocks the laser beam); 7. Control chamber (no laser); 7a. Control aerosol inlet; 7b Control aerosol outlet; 8. Cooling tank for control aerosol condensation. The real prototype is shown in **Supplementary** Fig. 3.

10^4 vg/cell and 10 iu/cell for AAV and LV vectors, respectively. For each dilution, we exposed the 1 μl drop to 2 s irradiation with the different laser wavelengths, as detailed in **Supplementary** Table 1. Again, we quantified both EGFP and Hoechst areas and calculated their ratio as an index of viral transduction activity. A reduction in this parameter indicates inactivation of the viral vector.

Results are shown in Fig. 1**c-f** for the lowest viral titer resulting in almost 100% cell transduction (1×10^6 vg/cell for AAV and 1×10^3 iu/cell for LV). As evident in the graphs of Fig. 1**c, d** and representative pictures in Fig. 1**e, f, 445** nm laser light significantly inhibited both AAV and LV transduction, being more effective on LV vectors, consistent with absorption of this wavelength by the lipid bilayer of the LV envelope. By diluting the viral preparations, this wavelength constantly inhibited LV activity by 75%, which resulted in complete LV inactivation at 1 iu/cell. Minimal activity of blue laser on AAV was observed at all dilutions, but never reached full inactivation (**Supplementary** Fig. 2). In contrast, 970 nm laser light had no or minimal effect on either vector type at all tested dilutions. The most striking results were obtained using MIR and NIR infrared wavelengths (10,600 nm and 1940 nm), which inactivated viral transduction by both vectors at all tested dilutions (**Supplementary** Fig. 2). These infrared lasers were effective even at a higher viral concentration (1×10^7 vg/cell for AAV and 1×10^4 iu/cell for LV). Since the 10,600 nm performed better than 1940 nm laser light and because of easier manufacturing and lower cost, it was therefore decided to continue experimentation with the longest 10,600 nm wavelength.

3.2. Generation of a new laser device capable of sterilizing human-like aerosol contaminated by lentiviral particles

It was of interest and importance to verify whether the 10,600 wavelength was able to inactivate viral particles, not only on a solid and static surface, but also in aerosol conditions. We used LV vectors, as they are closer in size and structure to most of respiratory viral pathogens. A 3 ml solution containing 5×10^6 iu/ml LV particles was nebulized, using two commercially available nebulizers, producing aerosol droplets exploiting ultrasounds and the Venturi effect, respectively. The generated aerosol was collected in a plastic tube kept on ice to allow condensation of the vector solution, as schematically represented in Fig. 2**a.** A drop (20 μl) of the condensed vector solution was eventually added to HEK293 cells. As shown in Fig. 2**b**, both aerosol systems inactivated LV particles.

As an aerosol containing active viral particles was necessary in order to evaluate the anti-microbial activity of laser light, we generated a nebulizer. Firstly, we produced the aerosol by using a vacuum pump connected to the liquid dispenser via a vacuum-resistant tube. The insertion of a valve within the tube allowed to tune the flow rate and to generate a gentle airflow. Even in this scenario, all viral particles were inactivated by the nebulization process (Fig. 2**b)**. We then further improved the system by modifying the commercially available nebulizer exploiting Venturi effect, as detailed in Material and Methods and Supplementary Material. As shown in Fig. 2**c**, in this system a 2 m long silicon tube acts as a low pass filter to keep the airflow at the inlet of the aerosol dispenser constant, thus producing a regular nebulization, attenuated in pressure, not exerting mechanical stress on microbial particles. In this case, the condensed liquid contained numerous infectious LV particles, allowing to preserve about 60% of the original viral activity (Fig. 2**b)**. We also assessed the microscopic appearance of the droplets, by placing a cell culture dish at 20 cm from the outlet of the aerosol generator and observing the droplets by bright field microscopy. As shown in Fig. 2**d, e**, most of the droplets were in the 5–80 μm diameter range and appeared very similar to those generated by a speaking person.

Having set up a system to generate an aerosol containing a high concentration of viable LV particles, we combined it with a close box in which to irradiate the generated aerosol with 10,600 nm laser light.

A schematic representation of this prototype is shown in Fig. 2**f** and its legend, which also includes a description of its multiple components. More experimental details of this prototype are provided in **Supplementary** Fig. 3and Supplementary Material.

3.3. MIR laser light effectively inactivates aerosolized viruses and bacteria

We next used our prototype to test whether 10,600 nm laser effectively inactivated aerosolized LV particles. As shown in Fig. 3 **a, b**, the control solution recovered from tank n. 8, which was not exposed to any laser beam, contained active LVs, able to efficiently transduce HEK293 cells, consistent with the results shown in Fig. 2**b**. In contrast, the solution recovered from tank n. 5, which was generated from an aerosol irradiated with 10,600 nm laser light for <15 ms, did not contain detectable active particles (Fig. 3**a, b**). It was concluded that ultra-rapid exposure to 10,600 nm laser light effectively inactivated LV particles in both static and aerosol conditions.

To validate the potential of this sterilizing system on human microbial pathogens, we first tested its efficacy on SARS-CoV-2 (Licastro et al., 2020). We again used our prototype to aerosolize a solution containing 6×10^5 pfu/ml of SARS-CoV-2. Consistent with the results obtained using LV vectors, nebulization per se did not significantly inactivate the virus (Table 1). We then assessed the effect of laser irradiation by recovering the condensed material from tanks n. 5 and n. 8, as described before. We quantified the recovered viral particles by plaque assay. As shown in Table 1 and Fig. 3**c**, irradiation with 10,600 nm laser light for <15 ms resulted in > 99% viral inactivation. The absolute number of SARS-CoV-2 pfu recovered before and after laser irradiation for three independent experiments is reported in Table 1.

Finally, it was of interest to assess whether the system was also effective on the airborne bacterial *L. pneumophila*. We repeated the experiment using a bacterial culture as a starting material for aerosol generation. Bacterial viability after nebulization and treatment with laser light was quantified by plating the recovered solutions on plate media at multiple dilutions. In this case, nebulization per se slightly reduced bacterial viability (Table 2). Yet, 10,600 nm laser light effectively inactivated most of the remaining bacterial cells in <15 ms, resulting with over 99% efficiency (Table 2 and Fig. 3**d**).

3.4. Implementation of the new technology into a real device

Based on the positive results obtained with both viruses and bacteria, we started transforming our prototype into a commercial device, which can be safely placed in a closed environment. Lasers are classified for safety purposes based on their potential for causing injury to human eyes and skin (American National Standard for Safe Use of Lasers, 2014; Safety of laser products, 2014). The CO_2 laser inserted in our system is classifiable as a class 4 product, meaning that it is hazardous under both intrabeam and diffuse reflection viewing conditions, it may cause skin injuries, and it represents a potential fire hazard. Yet, the final configuration of our device ensures that it remains fully enclosed, and that light cannot leak under normal use. Thus, the final device is classifiable as a class 1 product, as it is "very low risk and safe under reasonably foreseeable use" and it is exempt from all beam-hazard control measures.

A technical representation of the final air filtering device is shown in Fig. 4**a, b**. Air is sucked from the room into the laser sterilization chamber by a powerful fan, capable of aspirating up to 900 m^3/h of air. The fan is expected to run at variable speed depending on the presence of people in the room: 50 m^3/h in an empty room, to be increased to 150 m^3/h when people enter the room, as detected by dedicated sensors. In other words, in a space of 30 m^3, such as a small office or an elevator populated by people, the total air volume would be filtered 120 times in 24 h (5 times per h). This flow rate, associated with a 50 cm long sterilization chamber in the real device (compared to 7.5 mm in the prototype) will ensure an exposure time of 50 ms, much higher than the minimal time proven to effectively inactivate >99% microbial particles.

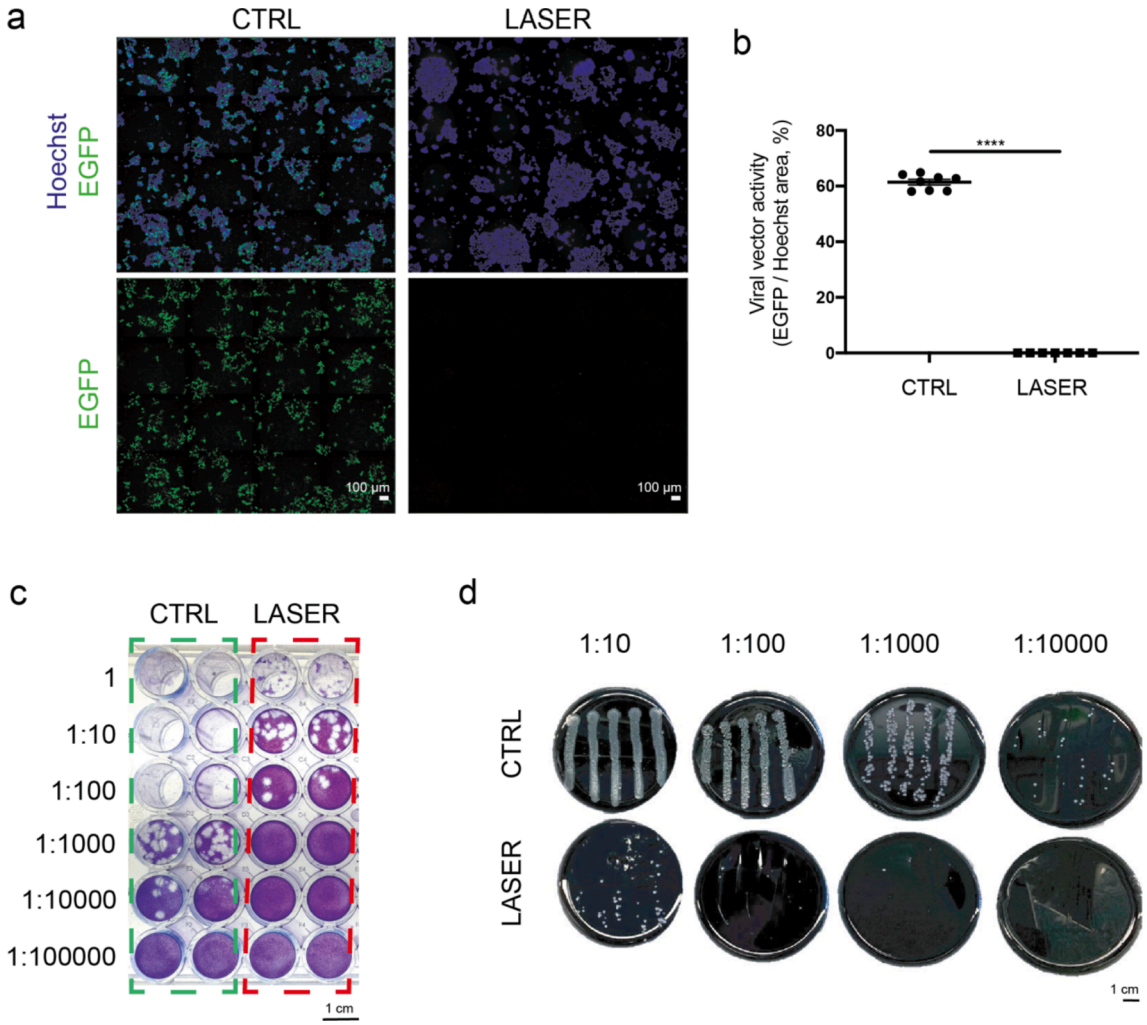

Fig. 3. Aerosolized viral vectors and human pathogens are efficiently inactivated by 10,600 nm laser light, a. Representative images of HEK293 cells infected with LV-EGFP at 48 h after infection. LV-EGFP was nebulized and irradiated using our prototype and condensed. Samples from tanks n. 8 (CTRL, control) and n.5 (laser-treated) were eventually added to cells. **b.** Quantification of LV activity, measured as EGFP/Hoechst area. The lower detection threshold in this assay is 10 LV-EGFP iu/cell. ****P < 0.0001. **c.** Representative images of cytopathic effect (white plaques) of SARS-CoV-2 on Vero cells in 48-well plates. Both control (CTRL, green dashed line) and laser-treated (red dashed line) samples were plated on Vero cells at multiple dilutions for quantification of plaque formation. **d.** Representative images of *L. pneumophila* colonies on Agar plates. Both control (CTRL) and laser-treated samples were plated on Agar at multiple dilutions for quantification of bacterial viability.

Sterilized air exits from the lateral sides of the fan, which is oversized to prolong its lifetime and minimize noise.

The sterilization chamber is a resonant optical cavity containing two plane mirrors, located at each extremity, at a 50 cm distance. These gold-coated mirrors almost completely (>99%) reflect 10,600 nm light. The laser beam (1.8 mm in size) enters the sterilization chamber through a small hole. Because of light diffraction, the laser beam bounces back and forth between the mirrors, progressively increasing in size during propagation. This results in a 75 mm beam diameter after 10 bounces, which exceeds the size of the chamber and thus ensures that the whole air volume is intercepted and sterilized by the propagating light.

Various formats of the device are represented in Fig. 4**c-f**. In particular, the device could hang either from the ceiling of a room, to be eventually hidden in a false ceiling (i.e. in airports, malls and hospitals, Fig. 4**c**) or installed in a lift (Fig. 4**d**). Alternatively, different set-ups could allow the positioning of the device close to people and even in between individuals, such as a pyramid standing on the floor of a dancing or sport room (Fig. 4**e**), or a tube hanging from a lateral wall in restaurants and offices (Fig. 4**f**).

Additional details on the real device are provided in Supplementary Material.

4. Discussion

Here we describe a new laser device able to neutralize two major human pathogens, SARS-CoV-2 and *L. pneumophila*. In this study, we also developed a new aerosol system in which microbes remain alive and able to infect permissive cells. Our data clearly indicate that the nebulization procedure per can significantly affect viral viability, largely depending on the method used to generate the aerosol droplets. Consequently, we have generated a nebulizer able to preserve the infectivity of viral particles, both of LV vectors and SARS-CoV-2, as well as bacterial cells. This relies on a constant airflow at the inlet of the aerosol dispenser with attenuated pressure, so that microbial particles are not inactivated by mechanical stress. This renders it rather unique in comparison to existing nebulizers for which the effect of aerosolization on viral and bacterial load has been tested using biochemical quantification of structural components of viral particles (either proteins or genomes), which not necessarily correlates with viability and infectivity (Zupin et al., 2021). When functional infectivity tests were performed, this showed that microbes were inactivated by aerosolization or in other cases, no quantitative results were numerated (Allegra et al., 2016; Fears et al., 2020; Smither et al., 2020; van Doremalen et al., 2020). Thus, our

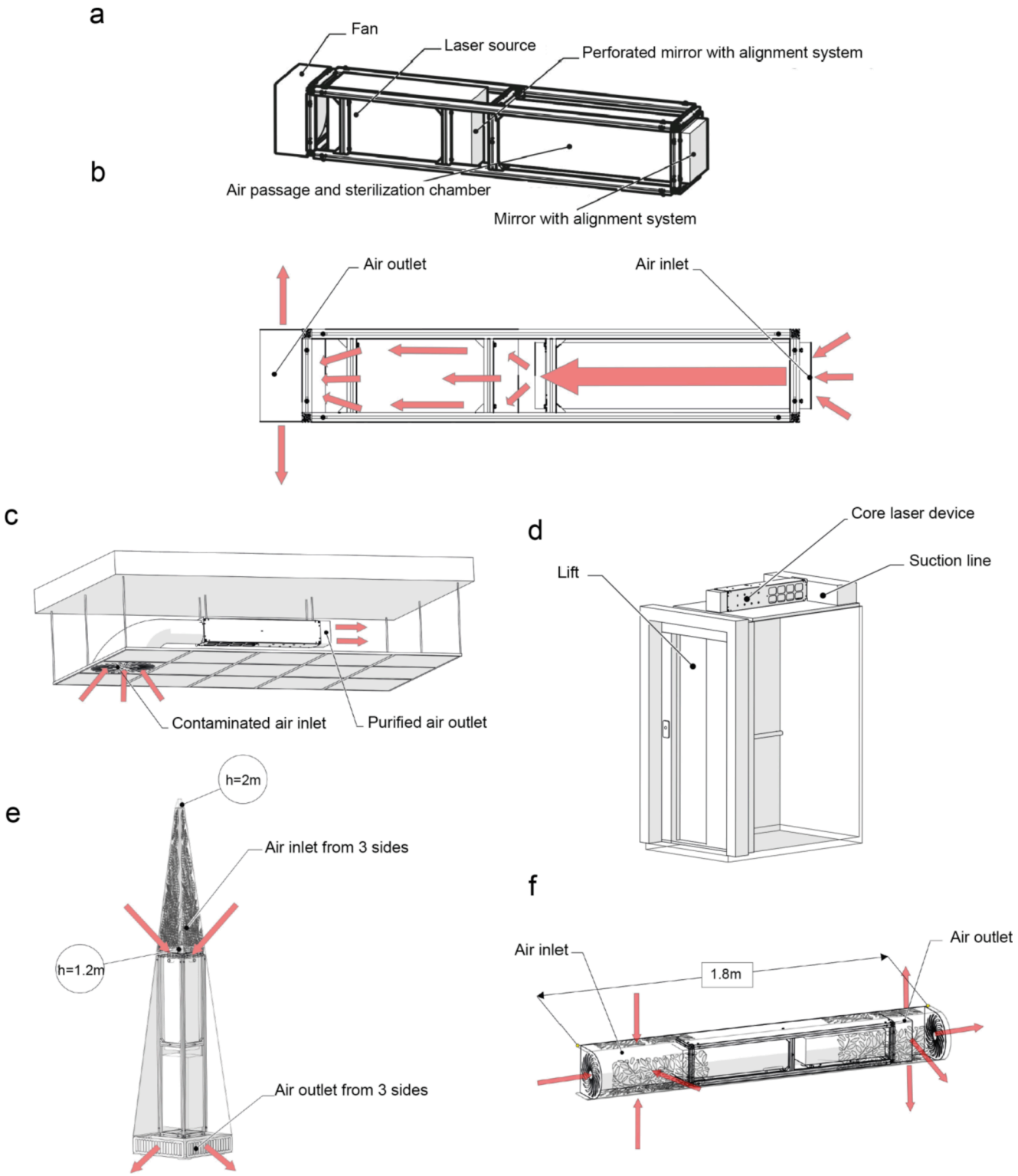

Fig. 4. Implementation of the new laser technology in real settings, a. Schematic drawing showing the core of the proposed laser technology, with indication of its major components. **b.** Schematic representation of air inflow and outflow from the core system. As indicated by the red arrows, the air is aspirated by the fan at the end of the system to enter the sterilization chamber, where it is exposed to laser light. Purified air exists from both sides of the fan. **c.** Schematic representation of a real device inserted into a false ceiling. Air flow is indicated by the red arrows. **d.** Schematic representation of a real device inserted into the ceiling of an elevator. **e.** Schematic representation of a real device designed to be placed in a populated room. Air flow is indicated by the red arrows. **f.** Schematic representation of a real device designed to be placed in a populated room, hanging from a lateral wall. Air flow is indicated by the red arrows.

system is unique in ensuring maintenance of the viability of viral vectors, coronaviruses, and bacterial cells.

The size of the liquid particles generated by the aerosol system reported here and that of a speaking person, was compared and similar distribution in the 5–200 μm range was detected, with the majority being lower than 80 μm. Importantly, recent evidence has demonstrated that 100 μm represents the largest particle size that remains suspended in air for >5 s and travels beyond 1 m from an infected person (Wang et al., 2021). Thus, droplet-spray deposition and aerosol inhalation represent the predominant ways of propagation of airborne transmitted diseases in indoor environments (Wang et al., 2021). While opening the window in a room can often remove the majority of these particles, there are situations in which ventilation is almost impossible (eg in elevators, airports, etc.) or inadequate to efficiently clean the air. The laser device reported here can provide a solution for these conditions, as it can be placed in an indoor environment and sterilize the air in real time. We present the efficacy of a prototype that exploits 10,600 nm laser light that can inactivate both bacterial and viral particles. After comparison of the activity of multiple wavelengths, it was determined that the 10,600 nm wavelength was the most effective against viruses and bacteria; in addition it is moderately cheap and easy to manufacture. Indeed, while other infrared laser technologies, emitting from 1940 to 3000 nm, are relatively bulky, complex and expensive, costing €30,000–50,000, CO_2 lasers, which emit at 10,600 nm, are simpler, more compact and reliable. The CO_2 laser incorporated in our device guarantees maintenance-free sealed-off performance with gas lifetime approaching 50,000 h. This significantly reduces both the initial investment and operational costs, making the 10,600 nm CO_2 laser an economically viable solution for air purification (estimated cost for each device: €1500–2000).

This specific wavelength is the highest absorption peak for the most common chromophores present in biological samples, including water, and thus exerts a high photothermal and photomechanical effect (Omi and Numano, 2014). Our data is consistent with for the destructive activity of the laser beam on aerosolized *L. pneumophila* and SARS-CoV-2. The mechanism of action for both microbes is currently unknown, it is consistent with previous evidence showing the anti-microbial effect of light (Rupel et al., 2019). This laser device can potentially also be a viable solution in the control of multi-drug resistant (MDR) bacteria, which are expected to determine over 10 million deaths every year (Klemm et al., 2018).

Our system presents advantages over the existing air sterilizing solutions which mostly rely on the use of HEPA filters, which mechanically entrap particles larger than a defined size; these can reach the market without the need of a biological test confirming their actual efficacy in blocking the diffusion of infectious microorganisms. The same is true for light-based sterilizers, which are also rarely certified using biological assays. Thus, the device of this study is uniquely validated for its capacity to inactivate both bacterial and viral particles responsible for major societal and sanitary problems.

Compared to existing light-based technologies, which usually require an exposure time of several minutes to achieve effective air or surface sterilization, our prototype acts in a very short time. We demonstrate here that exposure of aerosolized viral or bacterial particles to a 10,600 nm laser beam for <15 ms results in the inactivation of over 99% of microbes. This high performance is expected to become even more effective in the final device, in which the air will be repeatedly conveyed through a multiplicity of laser beams, progressively enlarged in size, for longer times.

Possible limitations of our device are failure of the laser system and either misalignment or damage of the mirroring system; both of these are rather low risks. The CO_2 laser is a mature and consolidated technology, invented over 50 years ago (Patel, 1964), and has a mean time between failures of 50,000 h, allowing for many years of operation without service. Similarly, while it is possible that the optical system gets misaligned or damaged by the laser itself, the design of the optical cavity is relatively simple and thus intrinsically robust. Mirrors are made to work far below the laser-induced damage threshold and alignment sensors with feedback actuators further ensure reliable alignment.

Importantly, the laser technology is more environmentally friendly compared to HEPA filters, UV lamp and other materials considered for air cleaning. HEPA filters generally have a short life, thus requiring regular replacement to prevent the reintroduction of airborne microorganisms into the environment (Niu et al., 2020). The same applies to UV lamps, which also need to be regularly replaced, increasing the costs. In addition, UV lamps have high energy consumption due to their relative inefficiency, never higher than 35%. These limitations have so far prevented their mass market adoption. It is therefore time for alternative strategies to be developed. Our system represents a novel solution for air cleaning, which is technically valid, experimentally validated, sustainable, robust by design and economically viable.

CRediT authorship contribution statement

Roman Vuerich: Conceptualization, Validation, Investigation, Formal analysis, Writing – original draft, Writing – review & editing. **Valentina Martinelli:** Validation, Formal analysis. **Simone Vodret:** Investigation. **Iris Bertani:** Investigation, Writing – original draft. **Tea Carletti:** Investigation, Writing – original draft. **Lorena Zentilin:** Resources. **Vittorio Venturi:** Resources, Writing – review & editing. **Alessandro Marcello:** Resources. **Serena Zacchigna:** Conceptualization, Validation, Formal analysis, Resources, Writing – original draft, Writing – review & editing, Supervision, Project administration, Funding acquisition.

Declaration of Competing Interest

The authors declare the following financial interests/personal relationships which may be considered as potential competing interests: Valentina Martinelli reports financial support was provided by Eltech K-laser srl. Valentina Martinelli reports a relationship with Eltech K-laser srl that includes: employment. Serena Zacchigna has patent pending to Licensee.

Acknowledgments

We are grateful to Marina Dapas, Michela Zotti for excellent technical support in viral vector production. Intramural funds from the ICGEB and liberal financial contribution to A.M. from Generali SpA, SNAM SpA, and Beneficentia Stiftung in the context of the COVID-19 emergency is hereby acknowledged.

Appendix A. Supplementary material

Supplementary data to this article can be found online at https://doi.org/10.1016/j.envint.2022.107272.

References

Allegra, S., Leclerc, L., Massard, P.A., Girardot, F., Riffard, S., Pourchez, J., 2016. Sci. Rep. 6, 33998. https://doi.org/10.1038/srep33998.

(a) American National Standard for Safe Use of Lasers ANSI Z136.1 Standard ed., 2014; (b) Safety of laser products - part I: equipment classification and requirements. IEC document 60825-1 ed.; 2014.

[3] Bono et al., 2021 Bono, N., Ponti, F., Punta, C., Candiani, G., 2021. Materials (Basel) 14, 5. https://doi.org/10.3390/ma14051075.Feng et al., 2017 Feng, Y., Liu, L., Zhang, J., Aslan, H., Dong, M., 2017. J. Mater. Chem. B 5 (44), 8631. https://doi.org/10.1039/c7tb01860f.Matsuura et al., 2021 Matsuura, R., Lo, C.W., Wada, S., Somei, J., Ochiai, H., Murakami, T., Saito, N., Ogawa, T., Shinjo, A., Benno, Y., Nakagawa, M., Takei, M., Aida, Y., 2021. Viruses 13 (5). https://doi.org/10.3390/v13050942.

Buffolo, M., De Santi, C., Norman, J., Shang, C., Bowers, J.E., Meneghesso, G., Zanoni, E., Meneghini, M., 2021. Electronics 10, 2734.

Buse, H.Y., Hall, J.S., Hunter, G.L., Goodrich, J.A., 2022. Microorganisms 10, 2. https://doi.org/10.3390/microorganisms10020352.

[6] Chikkaraddy et al., 2022 Chikkaraddy, R., Xomalis, A., Jakob, L.A., Baumberg, J. J., 2022. Light Sci. Appl. 11 (1), 19. https://doi.org/10.1038/s41377-022-00709-

8.Tsai and Hamblin, 2017 Tsai, S.R., Hamblin, M.R., 2017. J. Photochem. Photobiol. B 170, 197. https://doi.org/10.1016/j.jphotobiol.2017.04.014.
Eisenloffel, L., Reutter, T., Horn, M., Schlegel, S., Truyen, U., Speck, S., 2019. PLoS One 14 (11), e0225047. https://doi.org/10.1371/journal.pone.0225047.
[8] Eulalio et al., 2012 Eulalio, A., Mano, M., Dal Ferro, M., Zentilin, L., Sinagra, G., Zacchigna, S., Giacca, M., 2012. Nature 492 (7429), 376. https://doi.org/10.1038/nature11739.Zacchigna et al., 2018 Zacchigna, S., Martinelli, V., Moimas, S., Colliva, A., Anzini, M., Nordio, A., Costa, A., Rehman, M., Vodret, S., Pierro, C., Colussi, G., Zentilin, L., Gutierrez, M.I., Dirkx, E., Long, C., Sinagra, G., Klatzmann, D., Giacca, M., 2018. Nat. Commun. 9 (1), 2432. https://doi.org/10.1038/s41467-018-04908-z.
[9] Fasnacht and Polacek, 2021 Fasnacht, M., Polacek, N., 2021. Front. Mol. Biosci. 8, 671037. https://doi.org/10.3389/fmolb.2021.671037.Rupel et al., 2018 Rupel, K., Zupin, L., Colliva, A., Kamada, A., Poropat, A., Ottaviani, G., Gobbo, M., Fanfoni, L., Gratton, R., Santoro, M., Di Lenarda, R., Biasotto, M., Zacchigna, S., 2018. Oxid. Med. Cell Longev. 2018, 6510159. https://doi.org/10.1155/2018/6510159.
[10] Fears et al., 2020 Fears, A.C., Klimstra, W.B., Duprex, P., Hartman, A., Weaver, S. C., Plante, K.S., Mirchandani, D., Plante, J.A., Aguilar, P.V., Fernandez, D., Nalca, A., Totura, A., Dyer, D., Kearney, B., Lackemeyer, M., Bohannon, J.K., Johnson, R., Garry, R.F., Reed, D.S., Roy, C.J., 2020. Emerg Infect. Dis. 26, 9. https://doi.org/10.3201/eid2609.201806.Smither et al., 2020 Smither, S.J., Eastaugh, L.S., Findlay, J.S., Lever, M.S., 2020. Emerg. Microbes Infect. 9 (1), 1415. https://doi.org/10.1080/22221751.2020.1777906.van Doremalen et al., 2020 van Doremalen, N., Bushmaker, T., Morris, D.H., Holbrook, M.G., Gamble, A., Williamson, B.N., Tamin, A., Harcourt, J.L., Thornburg, N.J., Gerber, S.I., Lloyd-Smith, J.O., de Wit, E., Munster, V.J., 2020. N. Engl. J. Med. 382 (16), 1564. https://doi.org/10.1056/NEJMc2004973.
Gora, S.L., Rauch, K.D., Ontiveros, C.C., Stoddart, A.K., Gagnon, G.A., 2019. Water Res. 151, 193. https://doi.org/10.1016/j.watres.2018.12.021.
Hawkins, C.L., Davies, M.J., 2019. J. Biol. Chem. 294 (51), 19683. https://doi.org/10.1074/jbc.REV119.006217.
Kim, D.K., Kang, D.H., 2018. Appl. Environ. Microbiol. 84, 17. https://doi.org/10.1128/AEM.00944-18.
Klemm, E.J., Wong, V.K., Dougan, G., 2018. Proc. Natl. Acad. Sci. USA 115 (51), 12872. https://doi.org/10.1073/pnas.1717162115.
Licastro, D., Rajasekharan, S., Dal Monego, S., Segat, L., D'Agaro, P., Marcello, A., 2020. J. Virol. 94, 11. https://doi.org/10.1128/JVI.00543-20.
Lippi, M., Riva, L., Caruso, M., Punta, C., 2022. Materials (Basel) 15, 3. https://doi.org/10.3390/ma15030976.
Niu, M., Shen, F., Zhou, F., Zhu, T., Zheng, Y., Yang, Y., Sun, Y., Li, X., Wu, Y., Fu, P., Tao, S., 2020. Environ. Int.105878 142. https://doi.org/10.1016/j.envint.2020.105878.
Omi, T., Numano, K., 2014. Laser Ther. 23 (1), 49. https://doi.org/10.5978/islsm.14-RE-01.
(a) Ottaviani, G., Gobbo, M., Sturnega, M., Martinelli, V., Mano, M., Zanconati, F., Bussani, R., Perinetti, G., Long, C.S., Di Lenarda, R., Giacca, M., Biasotto, M., Zacchigna, S.,2013. Am. J. Pathol., 183 (6), 1747, https://doi.org/10.1016/j.ajpath.2013.09.003; (b) Ottaviani, G., Martinelli, V., Rupel, K., Caronni, N., Naseem, A., Zandona, L., Perinetti, G., Gobbo, M., Di Lenarda, R., Bussani, R., Benvenuti, F., Giacca, M., Biasotto, M., Zacchigna, S., 2016. EBioMedicine, 11, 165, https://doi.org/10.1016/j.ebiom.2016.07.028.
Pak, A., Adegboye, O.A., Adekunle, A.I., Rahman, K.M., McBryde, E.S., Eisen, D.P., 2020. Front. Public Health 8, 241. https://doi.org/10.3389/fpubh.2020.00241.
Pasanen, A.L., Keinanen, J., Kalliokoski, P., Martikainen, P.I., Ruuskanen, J., 1993. Scand. J. Work Environ. Health 19 (6), 421. https://doi.org/10.5271/sjweh.1452.
Patel, C.K.N., 1964. Phys. Rev.. 136 (5A), A1187.
Rajasekharan, S., Milan Bonotto, R., Nascimento Alves, L., Kazungu, Y., Poggianella, M., Martinez-Orellana, P., Skoko, N., Polez, S., Marcello, A., 2021. Viruses 13 (5). https://doi.org/10.3390/v13050808.
Ren, H., Koshy, P., Chen, W.F., Qi, S., Sorrell, C.C., 2017. J. Hazard Mater. 325, 340. https://doi.org/10.1016/j.jhazmat.2016.08.072.
Rupel, K., Zupin, L., Ottaviani, G., Bertani, I., Martinelli, V., Porrelli, D., Vodret, S., Vuerich, R., Passos da Silva, D., Bussani, R., Crovella, S., Parsek, M., Venturi, V., Di Lenarda, R., Biasotto, M., Zacchigna, S., 2019. NPJ Biofilms Microbiomes 5, 29. https://doi.org/10.1038/s41522-019-0102-9.
Rupel, K., Zupin, L., Ottaviani, G., Bertani, I., Martinelli, V., Porrelli, D., Vodret, S., Vuerich, R., Passos da Silva, D., Bussani, R., Crovella, S., Parsek, M., Venturi, V., Di Lenarda, R., Biasotto, M., Zacchigna, S., 2019. NPJ. Biofilms Microbiomes 5 (1), 29. https://doi.org/10.1038/s41522-019-0102-9.
Smijs, T.G., Pavel, S., 2011. Nanotechnol. Sci. Appl. 4, 95. https://doi.org/10.2147/NSA.S19419.
Volker, J., Stapf, M., Miehe, U., Wagner, M., 2019. Environ. Sci. Technol. 53 (13), 7215. https://doi.org/10.1021/acs.est.9b00570.
Wang, C.C., Prather, K.A., Sznitman, J., Jimenez, J.L., Lakdawala, S.S., Tufekci, Z., Marr, L.C., 2021. Science 373, 6558. https://doi.org/10.1126/science.abd9149.
Wang, H., Zhang, L., Luo, H., Wang, X., Tie, J., Ren, Z., 2019. Appl. Environ. Microbiol. 86, 1. https://doi.org/10.1128/AEM.01907-19.
Zacchigna, S., Marcello, A., Banks, L., 2021. FEBS J. 288 (17), 4992. https://doi.org/10.1111/febs.16167.
Zupin, L., Licen, S., Milani, M., Clemente, L., Martello, L., Semeraro, S., Fontana, F., Ruscio, M., Miani, A., Crovella, S., Barbieri, P., 2021. Int. J. Environ. Res. Public Health 18, 21. https://doi.org/10.3390/ijerph182111172.